Review of TPC detector R&D for MOST-CEPC Project
IHEP, Beijing, June 16, 2018

The International Review Committee listed below asked to review preliminary designs, R&D progress and some preliminary test results of TPC detector for MOST project.

This R&D effort is funded by the National Key Program for S&T Research and Development (Grant No. 2016YFA0400404), Ministry of Science and Technology of China in 2016-2021. The committee is specifically asked to review and comment on the following aspects related to the attached documents.

Members of the International Review Committee:

Ron Settles (MPI, Germany)
Roy Aleksan (Saclay, France)
Akira Sugiyama (SAGAU, Japan)
Ye Jingbo (SMU, USA)
Li Yulan (THU, China)
Li Xiaomei (CIAE, China)
Zhu Chengguang (SDU, China)

International Review of MOST Detector R&D Project

(2016YFA0400404)

IHEP, Beijing, June 16, 2018

Please choose the appropriate grade (mark √) for the following items based on your best knowledge (5 means the highest score, 1 means the lowest score):

Item 1: Does the detector design appear reasonable aiming to goals of the MOST project?

Answer: ⑤ ④ ③ ② ①

Item 2: Is the chosen technology option suitable for detector design with in MOST project?

Answer: ⑤ ④ ③ ② ①

Item 3: Does the current progress and preliminary test performance look promising ?

Answer: ⑤ ④ ③ ② ①

Item 4: Overall detector R&D performance in the past two years ?

Answer: ⑤ ④ ③ ② ①

Signature of International Review Committee:

Review report (attached below) :

Introduction of TPC detector R&D for MOST-CEPC project

The discovery of a SM Higgs boson at 125GeV at the LHC brought about great opportunity to investigate the feasibility of a Circular Electron Positron Collider (CEPC) operating at center-of-mass energy of $\sqrt{s}$~240 GeV, as a Higgs factory, with designed luminosity of about $2\times10^{34}cm^{-2}s^{-1}$. The CEPC provides a much cleaner collision environment than the LHC, it is ideally suited for studying the properties of Higgs boson with greater precision. Another advantage of the CEPC over the LHC is that the Higgs boson can be detected through the recoil mass method by only reconstructing Z boson decay without examining the Higgs decays. This method can make absolute measurement of Higgs decay branching ration possible. It also provides the best probe into the Higgs invisible decays and search for dark matter and exotic particles produced in the Higgs decays. The CEPC can also operate at the Z pole and near the WW threshold to allow for refined measurement of the SM parameters with significantly higher precision.

The circumference of CEPC is 100km, with two interaction points available for exploring different detector design scenarios and technologies. Two common RF stations are deployed for the Higgs operation, which result in 286 beam bunches evenly distributed over a half ring. While for W and Z operations, independent RF cavities are used, 5220 and 10900 bunches are spreading in equal distance over the full ring, respectively. Therefore, the bunch spacing are about 500ns, 50ns and 30ns for Higgs, W and Z operations, respectively.

The baseline design of CEPC detector is an ILD-like concept, with a superconducting solenoid of 3.0 Tesla surrounding the inner silicon detector, TPC tracker detector and the calorimetry system. In order to accommodate the CEPC collision environment, some necessary changes have been made to the Machine Detector Interface (MDI) and sub-detector design. The CEPC design, for instance, has a significantly shorter focal length L* of 2.2m than that of the ILC design (3.5m), which indicates that the final focusing magnet QD_0 will be placed inside the CEPC detector. In addition, unlike the ILC detector, the CEPC detector will operate in continuous mode, which imposes special considerations on power consumption and subsequent cooling of the sub-detectors.

The detector volume of preliminary Conceptual Design Report (Pre-CDR) was published in 2015[1], based on the single-ring machine designed with 54 km in circumference. The CDR with different MDI scheme and beam structure will be published in 2018 which is based on the fully partial double-ring design with 100km in circumference.

Aiming for the CDR and TDR of the CEPC project, two-phase funding scheme is proposed by the funding agency, the Ministry of Science and Technology (MOST) of China. To launch the project, the MOST funded the CEPC accelerator and detector R&D project for phase-I period of 2016-2021. Among sub-detectors, the feasibility study of the TPC tracker detector was initiated

for the purpose to identify feasible technology options and to gain expertise to build the detector units which meet the basic requirements of the CEPC detector design. The specific research goals of this MOST project are described as following.

● Progress of TPC tracker detector R&D for MOST-CEPC project

1. R&D on TPC detector module by MOST project (2016.7-2021.7)

Motivation:

Time Projection Chambers (TPCs) have been extensively studied and used in many fields, especially in particle physics experiments, including STAR [1] and ALICE [2]. Their low material budget and excellent pattern recognition capability make them ideal for three dimensional tracking and identification of charged particles. The TPC detector will operate in continuous mode on the circular machine. To fulfill the physics goals of the future circular collider and meet Higgs/Z run, a TPC with excellent performance is required. MPGDs with outstanding single-point accuracy and excellent multi-track resolution are needed. We have proposed and investigated the ions controlling performance of a novel configuration detector module. The aim of this study is to suppress ion backflow (IBF) continually.

Objectives:

The TPC detector at the proposed circular collider will have to be operated continuously and the backflow of ions must be minimized without the open/close time of a gating device technology. The gain of the selection detector module can be achieved up to about 5000 without any obvious discharge behaviour. The currents on the anode and drift cathode were measured precisely with an electrometer. The experimental results showed that IBF can be reduced to -0.1% at the gain of about 5000.

Progress and highlights:

1.1 The continuous IBF suppression TPC module of GEM-MM

There has been a critical problem with TPC detector, especially in high background conditions – the space charge distortion due to the accumulation of positive ions in the drift volume. Due to their large mass, positive ions move slowly under the action of electric field in the drift volume of the TPC. The continuously superimposed ions in the drift volume of the TPC may affect the drift behaviour of electrons from a later track. The majority of ions inside the drift volume are back flowing ions from the amplification region of the TPC readout

devices. It is thus of great importance to limit ion backflow from the amplification region. Early TPCs were equipped with multi-wire proportional chambers (MWPCs) as gas amplification devices. The IBF ratio in a standard MWPC is 30-40%[2], so a gating GEM is essential to prevent ions from reaching the drift volume. But it's Z pole run mode in the circular machine, there is the not enough the open/close time for this technology option.

The idea of combining GEM with Micromegas was first proposed with the goal of reducing the spark rate of Micromegas detectors. Pre-amplification using GEM also extends the maximum achievable gain, so there have also been studies on gaseous photomultipliers with this hybrid configuration. The cascaded structure of the GEM-MM detector is composed of a drift electrode, a GEM foil, a standard Micromegas, and a readout printed circuit board. The Micromegas detector is based on the bulk method and has an active area of 100mm×100mm. The micromesh is made of stainless steel wires 22μm in diameter, interwoven at a pitch of 62μm. 128μm under the micromesh is a single copper pad readout plane. A GEM foil is cascaded above the micromesh at a distance of 1.4mm. It is a standard GEM foil of area 100mm×100mm, produced from CERN. In the experiment, the drift distance was maintained at 4mm. Electrodes were biased with CAEN N471A high voltage units.

^{55}Fe source was used to produce the primary electrons in the sensitive volume during the test. The working gas was a mixture of Ar/CO_2(90/10) and T2K gas at room temperature and atmospheric pressure. Ion backflow is due to secondary ions generated in an electron-avalanche process in the amplification which return to the drift space. In this paper, fractional ion feedback is defined as the ratio of the ion charge injected into the drift volume, collected on the drift electrode, and the electron charge collected on the anode pad. A Keithley (6517B [3]) pico current electrometer device was used to measure the current with a resolution of -1.0pA.

1.2 Energy spectrum with GEM-MM detector

^{55}Fe X-ray source with a characteristic energy of 5.9keV was used in the test. In the argon-based working gas mixture, a typically pulse height spectrum for a GEM or Micromegas detector contains one major peak corresponding to the 5.9keV X-rays and an escape peak at lower pulse heights corresponds to the ionization energy of an electron from the argon K-shell. In the GEM-MM detector, the situation is different. There are two amplification stages inside this detector. The primary ionization created by photon absorption can be in the drift region or in the transfer region (Fig. 1). Photoelectrons starting from the drift region get amplified by both the GEM detector and the Micromegas detector before they are collected on the anode. If the photons are absorbed in the transfer region, the primary electrons will be amplified only once (by Micromegas).

Fig. 1 depicts a typical 55Fe pulse height spectrum obtained by the GEM-MM detector. Four peaks are seen in the pulse height spectrum. From left, the first peak and the second

peak are the escape peak and the full energy peak of the standalone Micromegas. The last two peaks are created by photons with their energy deposited in the drift region. These primary electrons show combination amplification. The principle of the GEM-MM detector is fully verified.

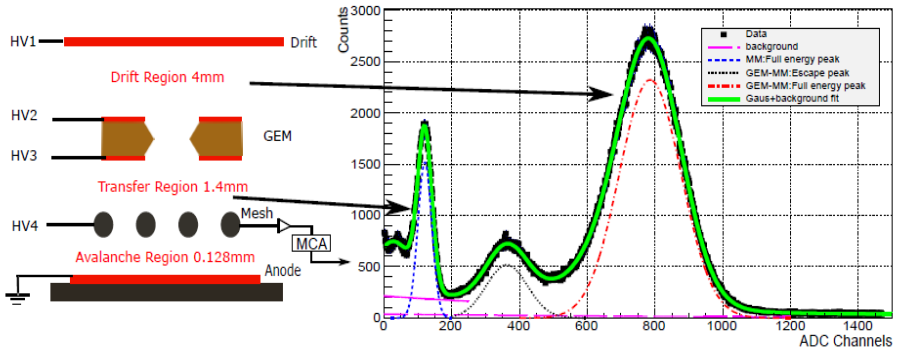

Fig.1 GEM-MM configuration (left) and pulse height spectrum at 5.9 keV for a GEM-MM, showing each peak and the corresponding location of primary ionization (right). Source: ^{55}Fe; Gas: Ar(90)+CO2(10);E_d=250V/cm, V_{GEM}=340V, E_t=500V/cm, V_{mesh}=420V.

1.3 Gain

With the calibrated electronic gain results, the gain of the detector is obtained from the measured spectra as described in the previous subsection. The gain of the Micromegas, GMM, is characterised by the first full energy peak in the spectrum. The last full energy peak represents the overall gain of the GEM-MM detector. It is important to note that this is a new way to measure the effective gas gain of a GEM. A gain of 5000 or more can be achieved without any obvious discharge behaviour.

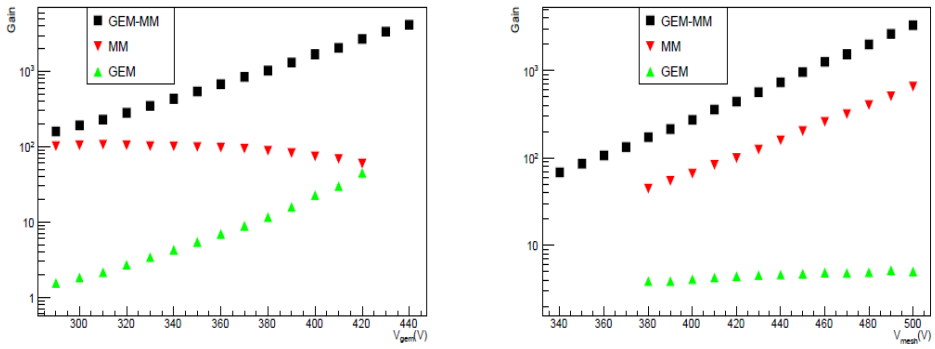

Fig.2 Gas gain versus GEM voltage, for micromesh V_{mesh}=420V (a) and micromesh voltage, V_{GEM}=340V (b). E_d=250V/cm, E_t=500V/cm.

The new gain results shows in Fig3 and the gain of GEM-MM detector operated in the two

different mixture gas of T2K and Ar/iC_4H_{10} respectively.

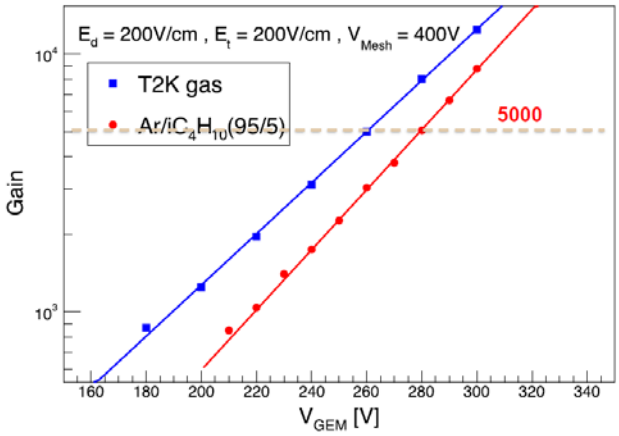

Fig.3 Gas gain at the mixture operation gas of T2K and Ar/iC_4H_{10}

1.4 Ion Backflow

IBF increases initially and decreases afterwards as the GEM voltage increases. So, an ion backflow value of -3% is considered to be the IBF for a standalone Micromegas detector with a gain of about 600. When the GEM is cascaded, the IBF can be further reduced to below 1%. Fig. 4 shows that when a constant bias voltage is set across the GEM, the IBF decreases as the micromesh voltage increases. The reason is that electrons collected on the anode increase with the increase of the mesh voltage. So the IBF can be estimated as a few percent for a single GEM detector with a comparatively low gain of approximately 4. After the Micromegas is cascaded, however, IBF is reduced significantly. An IBF ratio of 0.19% under overall detector gain of 5000 was achieved in our test in2017.

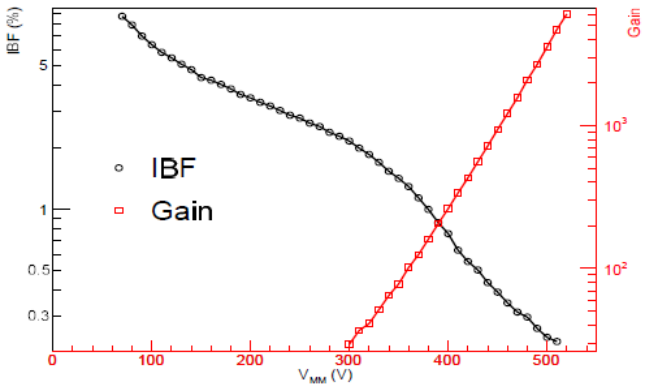

Fig.4 Gas gain and IBF versus
V_{GEM} = 340V. E_d = 250V/cm, E_t = 500V/cm@2017

In 2018, the parameters of the electric field of drift, transfer, GEM detector and Micromegas detector have been optimized testing. The key factor of the gas gain times IBF obtained at the mixtures gases of T2K and Ar/iC_4H_{10} separately. The new results has been shown in Fig. 5 and

some test parameters were given. To meet the Z pole run mode in the circular machine, some preliminary results of the simulation and estimation have been done in the publication paper [4].

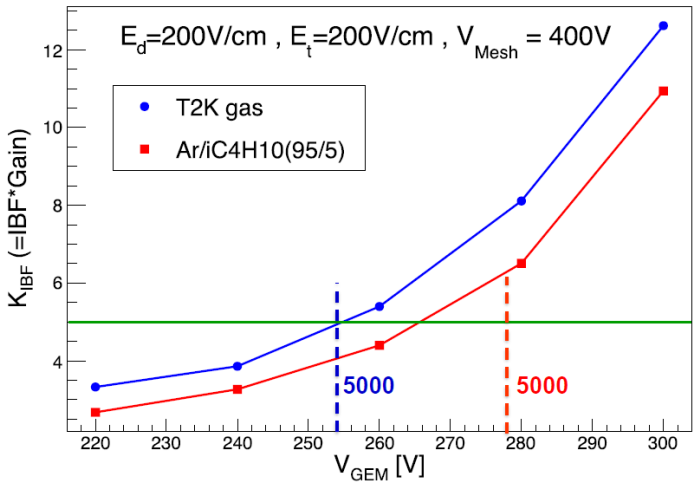

Fig.5 Factor of the gas gain and IBF@2018

2. R&D on the low power TPC front-end ASIC by MOST project (2016.7-2021.7)

Motivation:

Small readout pads of a few square millimeters (e.g. 1mm x 6mm) are needed to achieve high spatial and momentum resolution in TPC, demanding about 1 million channels of readout electronics per endcap. The total power consumption of the front-end electronics is limited by the cooling system to be several kilo-watts in practice and they have to work continuously in CEPC. Hence the technique of so-called power pulsing cannot be applied. There are no current existing electronics readout system can fulfill the requirements of such high density and low power consumption, including ALTRO/S-ALTRO and more recently SAMPA for ALICE, AFTER/GET for T2K and Timepix for ILC.

Objectives:

To develop a low power and highly integration front-end ASIC with direct waveform sampling in 65nm CMOS, the each channel consists of the analog front-end (AFE), including a charge sensitive preamplifier and a CR-RC shaper, and a waveform sampling ADC in 10b and 40 MSPS. The power consumption is less than 5mW per channel.

Progress and highlights:

2.1 The architecture and the key specification of the front-end ASIC

The readout electronics for CEPC TPC is shown in Fig.6. The front-end electronics has to be mounted on the endplate of the detector and hence needs to be very low power consumption. The waveform sampling is preferable for TPC signal processing due to the wide variation of the signal width. Several tens of Mega-Sample per Second (MSPS) is needed for drift time measurement. Digital signal processing and data compression are usually implemented as well. However only the development of low power analog front-end and the ADC will be focused in the MOST project and their specifications are listed in Table1.

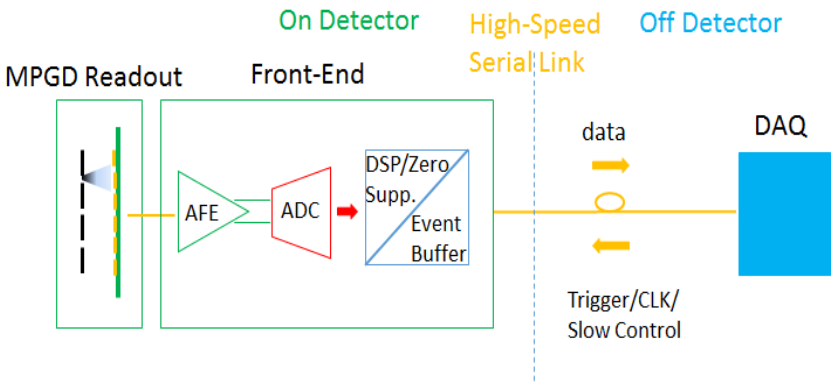

Fig.6 The architecture of the TPC readout electronics

Tab.1 The specifications of the front-end ASIC

Total number of channels		1 million per endcap
AFE	ENC	500 e @ 10pF input cap.
	Gain	10 mV/fC
	Dynamic Range	120fC
	Shaper	CR-RC
	Peaking time	160 ns
	INL	<1%
	Crosstalk	<1%
ADC	Sampling rate	Up to 40 MSPS
	Resolution	10 bit
	DNL	<0.6 LSB
	INL	<0.6 LSB
	ENOB	>9 bit
Power consumption		≤5mW per channel
Process		TSMC 65nm LP

2.2 Prototype chip design and test results

Three prototype chips were designed for our first MPW run, including a 5-channel analog front-end, a SAR (Successive Approximation Register) ADC and a 3-channel full function chips. The block diagram of the analog front-end and the SAR-ADC are shown in Fig.7 and Fig.8 respectively.

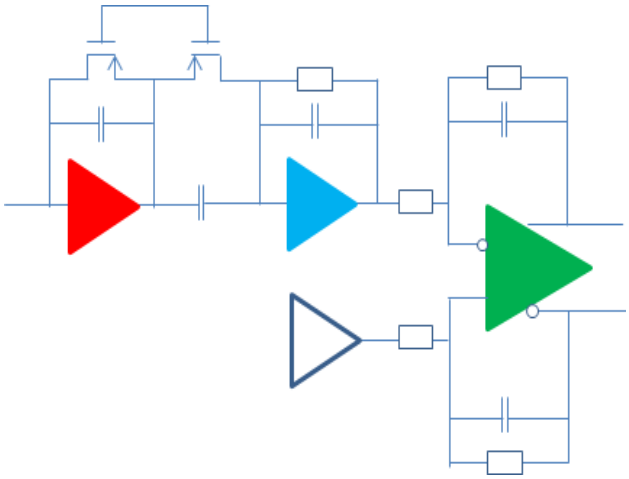

Fig.7 The block diagram of the analog front-end

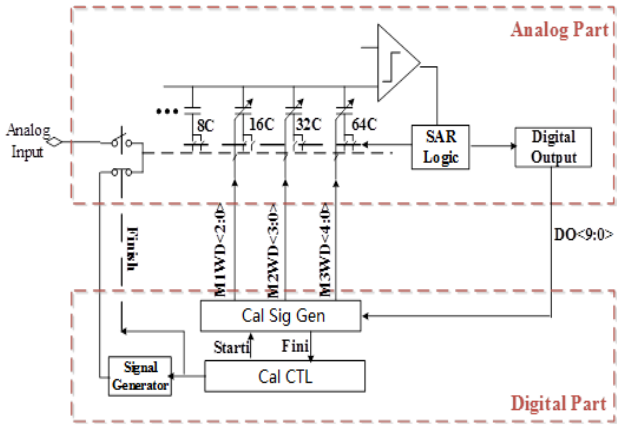

Fig.7 The block diagram of the SAR-ADC

The analog front-end and the SAR ADC chips have been evaluated and the test results are present below:

2.2.1 Test results of the analog front-end

The currents of the power supply were measured adjusting the master bias current. The power consumption of the analog front-end was estimated to be 2.18mW per channel at 25 μAbias current. All the other tests were done under this bias condition. The test setup and the transient output waveforms are shown in Fig.9. The peaking time of the output was 160ns.

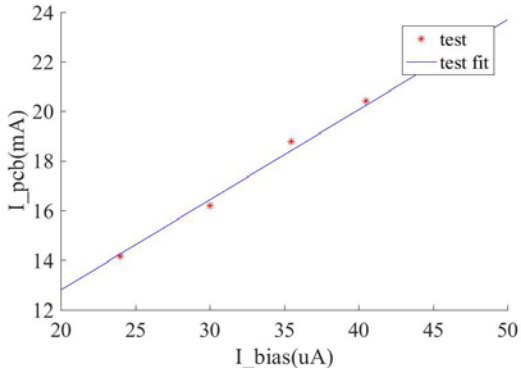

Fig.9 Power consumption with different bias current

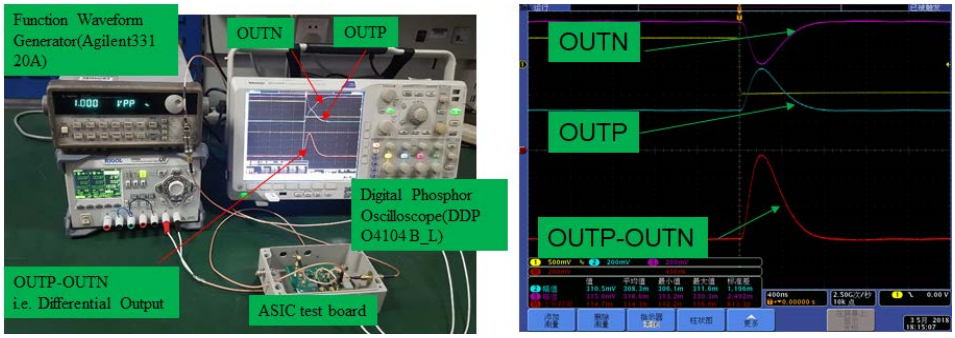

Fig.10 Test setup for the analog front-end (left) and the output waveforms (right)

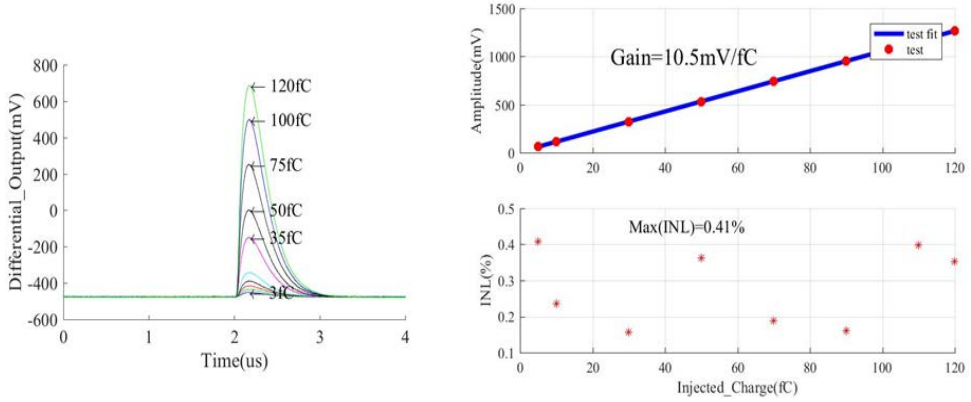

Fig.11 The output waveforms (left) and the linearity fitting (right)

The output signal waveforms injected with different input charge are show in Fig.11 and the gain and the linearity were estimated by linear fitting the signal amplitudes with the input charge. The gain was estimated to be 10.5mV/fC and the maximum INL was less than 0.41%.

The ENC noises were measured with different input capacitances, as shown in Fig.12. The fitted noise was 13.5 e/pF+313.7e.

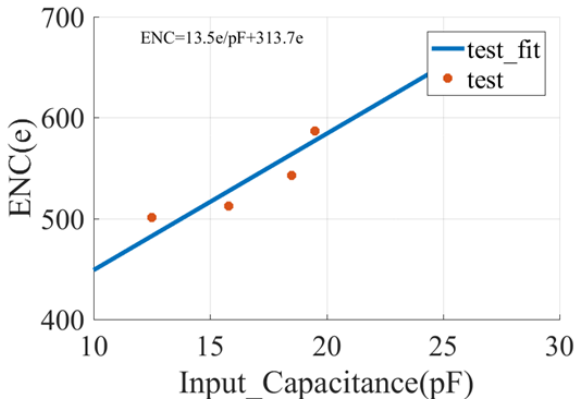

Fig.12 The measured ENC for different input capacitances

The crosstalk was measured by injecting signal into channel 3 and measuring the output of channel 2 and channel 1. The crosstalk was defined as:

$$\text{crosstalk} = \frac{\sqrt{A_{sn}^2 - A_{nn}^2}}{\sqrt{A_{si}^2 - A_{ni}^2}} \times 100\%$$

where A_{sn} and A_{si} are the peak-to-peak amplitudes of the neighboring and the injected channels and A_{nn} and A_{ni} are the noise variances in rms of the neighboring and the injected channels. The crosstalk$_{3\text{-}2}$ was measured to be 0.36% and the crosstalk$_{3\text{-}1}$ was 0.28%. The crosstalk from the charge injection circuits was included.

The test results of the analog front-end were compared with the specifications, as listed in Tab.2. All the design requirements were well met.

Table 2 Comparison of the specifications and the test results of the AFE

	Specifications	Test
Gain	10mV/fC	10.5mV/fC
Dynamic Range	120fC	120fC
Peaking time	160 ns	160 ns
INL	<1%	0.41%
Power consumption	<2.50mW/ch	2.18mW/ch
ENC	500e @ 10pF	448e @ 10pF
Crosstalk	<1%	0.36%

2.2.2 Test results of the SAR ADC

The test setup for the SAR ADC is shown in Fig.8. The chip was mounted in the evaluation PCB. The input sine signal of 2.4 MHz was used and the ADC output was recorded by the TI-TSW1400 data capture board. The measured INL and DNL are shown in Fig.14. With on-chip calibration, the maximum INL and DNL were less than 0.5 LSB. The measured SNR and SNDR are shown in Fig.10. The SNDR of 57dB was achieved, equivalent to an ENOB of 9.18 bit.

The power consumption of the SAR ADC core was estimated to be 1mW per channel at 50 MSPS sampling rate. The power consumption distributions among other circuit modules are also listed in Tab.3. For multi-channel design, the reference buffer and clock generator can be shared by all channels. Hence only the power consumption of the core circuit will be increased proportionally.

The test results of the SAR-ADC were compared with the specifications, as listed in Tab.4. All the design requirements were well met.

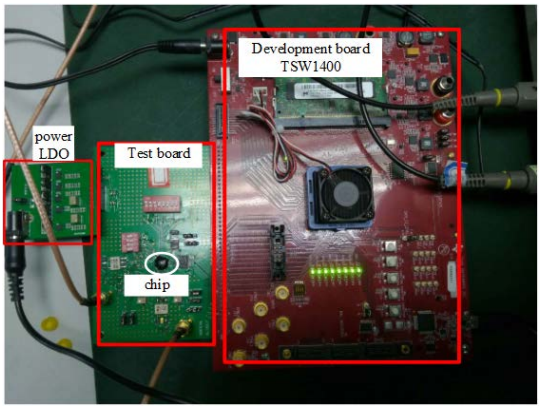

Fig.13 Test setup for the SAR ADC

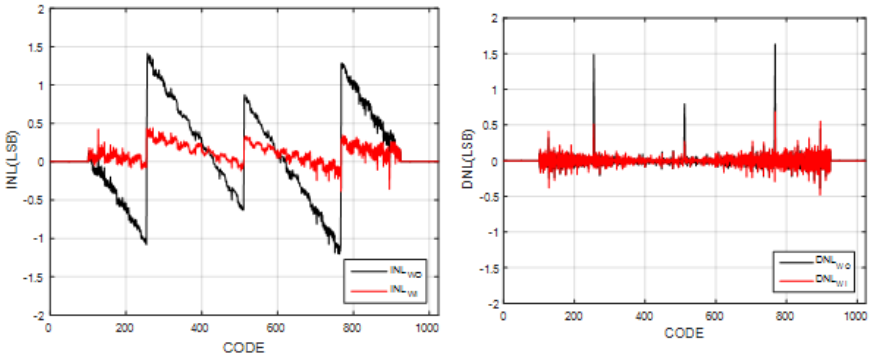

Fig.14 The measured INL (left) and DNL (right) with and w.o. calibration

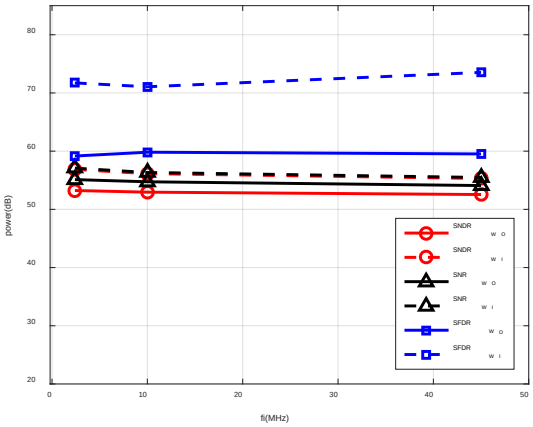

Fig.15 The measured SNR and SNDR (SINAD)

Table 3 Power consumption distribution in SAR ADC

Module	Power consumption （mW）
Total	4.0
Reference buffer	0.25
SAR ADC core	1.0
Others (CLK generator)	2.75

Table 4 Comparison of the specifications and the test results of the SAR ADC

	Specifications	Test
Sampling rate	40 MSPS	50 MSPS
Resolution	10 bit	10 bit
INL	<0.65 LBS	<0.5 LSB
DNL	<0.6 LSB	<0.5 LSB
ENOB	>9 bit	9.18 bit
Power consumption	<2.5 mW/ch	1mW/ch

References:

[1] http://cepc.ihep.ac.cn/preCDR/volume.html

[2] W. Blum, G. Rolandi, Particle Detection with Drift Chambers, Springer-Verlag, Berlin (1993)

[3] Keithley Instruments Inc., Model 6517B Electrometer Reference Manuel, 6517B-901-01 Rev. B, Cleveland, June (2009)

[4] Zhao M, Ruan M, Qi H, et al. Feasibility study of TPC at electron positron colliders at Z pole operation[J]. Journal of Instrumentation, 12.07 (2017)